Thermally Stimulated Current Analysis of Defects in Sol–Gel Derived $SrTa_2O_6$ Thin-Film Capacitors

Japanese Journal of Applied Physics **51** (2012) 09LA18 **REGULAR PAPER**
http://dx.doi.org/**10.1143/JJAP.51.09LA18**

Thermally Stimulated Current Analysis of Defects in Sol–Gel Derived $SrTa_2O_6$ Thin-Film Capacitors

Li Lu[1], Takashi Nishida[1,2], Masahiro Echizen[1], Yasuaki Ishikawa[1,2], Kiyoshi Uchiyama[3], Tadashi Shiosaki[4], and Yukiharu Uraoka[1,2]

[1]*Graduate School of Materials Science, Nara Institute of Science and Technology, Ikoma, Nara 630-0192, Japan*
[2]*CREST, Japan Science and Technology Agency, Kawaguchi, Saitama 332-0012, Japan*
[3]*Tsuruoka National College of Technology, Tsuruoka, Yamagata 997-8511, Japan*
[4]*Shibaura Institute of Technology, Koto, Tokyo 135-8548, Japan*

Received May 24, 2012; accepted June 25, 2012; published online September 20, 2012

In this research, we demonstrated that defect states in sol–gel-derived $SrTa_2O_6$ (STA) thin films can be detected by a thermal simulated current (TSC) technique. We also tentatively explained leakage current properties using these defect states. Similar defect states were found in STA thin films that were annealed at 700 and 800 °C by the TSC technique. Defects that caused the TSC peak at measurement temperatures of 130–150 °C showed higher trap densities in the 800 °C-annealed STA thin film. These defects were likely to be caused by diffused Ti, which mainly contributed to the larger leakage current in the 800 °C-annealed STA thin film. Oxygen-vacancy-related defect states were also clearly observed with the change in measurement atmosphere from air to vacuum.

1. Introduction

The rapid shrinking of electronic devices, such as dynamic random access memories (DRAMs), embedded capacitors, and metal–oxide–semiconductor field-effect transistors (MOSFETs), requires the development of dielectric materials for replacing SiO_2 to achieve a high dielectric constant (ε_r) and a low leakage current.[1–16] The use of tantalum pentoxide (Ta_2O_5) as a high-k material has often been reported because of its relatively high ε_r values of about 20–50.[2–6] However, these ε_r values are still inadequate for further miniaturization. A Sr-doped Ta_2O_5, $SrTa_2O_6$ (STA), which shows a much higher ε_r, is regarded as a promising candidate.[10–16] In our previous work, we also fabricated STA thin films with high ε_r values of about 26–140 and low leakage currents using a sol–gel method.[17–19]

The sol–gel method is a very simple method of fabricating dielectric and semiconductor thin films. It has many advantages including production of films with good homogeneity, low equipment cost, and easily compositional control of multicomponent materials.[20,21] However, sol–gel-derived thin films usually show weaker electrical properties than other vacuum-process-derived thin films. Carbon (C) and hydrogen (H) impurities, which originate from the organic precursor, are often considered as one of the main reasons why leakage current properties deteriorate. For sol–gel-derived STA thin films, the remaining C and H or other impurities, such as Ti, which was found in our previous work, were expected to play an important role in leakage current.[17,22] In order to improve electrical properties, defect states in STA thin films should be elucidated. Since no detailed defect analysis of sol–gel STA thin films has been reported until now, we adopted the thermal simulated current (TSC) technique to investigate defect states. The TSC technique is a simple and nondestructive method of studying defect states in semiconductor and insulators.[23–25]

2. Experimental Procedure

The STA sol–gel precursor (Mitsubishi Material) used had a composition of Sr : Ta = 1 : 2 and a metal alkoxide concentration of 7 wt %. The prepared precursor was spin-coated onto $Pt/TiO_2/SiO_2/Si$ substrates at 3000 rpm for 30 s. The TiO_2 layer was used to improve the adhesion between the electrode and the SiO_2/Si substrate.[26] After spin coating, the deposited thin films were dried at 100 °C for 5 min and pyrolyzed at 450 °C for 4 min on hot plates in air. The coating and heat treatment procedures were performed several times until the thin films were about 150 nm thick. Then, the thin films were annealed in O_2 at 700 (STA-700) and 800 °C (STA-800) for 1 h.

The thickness of the deposited films was determined by scanning electron microscopy (SEM; JEOL JSM-6301F). The depthwise distribution of the elements was analyzed by secondary ion microprobe mass spectrometry (SIMS; Ion-Microprobe Atomika-6500) using a Cs ion beam. The refractive index (n) of the fabricated STA thin films was measured by spectroscopic ellipsometry (HORIBA Jobin Yvon UVISEL ER AGMS-NSD). Leakage current was measured with a programmable electrometer (Keithley 617). A hold time of 20 s was set for each measurement point to eliminate the effect of relaxation processes.

The TSC of the capacitor with a Pt/STA/Pt structure was measured. Pt top electrodes of about 0.1 mm diameter were prepared with a shadow mask using rf sputtering. In order to measure the TSC, the film capacitor was set on a heater stage and connected to a programmable electrometer (Keithley 6517) by a Pt wire. Measurement atmospheres of vacuum with an atmospheric pressure of about 10 Pa and air were used. In order to observe clear TSC peaks, various poling voltages (V_p) and collection voltages (V_c) were investigated. V_p and V_c were finally set at ±0.3 and ±0.01 V for STA-700, and ±0.1 and 0 V for STA-800, respectively. $+V_p$ means that a positive V_p was applied to the bottom Pt electrode. The measurement temperature was set from room temperature (RT) to 300 °C with a heating rate of 2 °C/min. The measurement profile is shown in Fig. 1. Detailed measurement information was reported in ref. 24. In order to understand whether or not the electrical properties of thin films would deteriorate at high measurement temperatures, the dielectric properties of all thin films were measured twice from RT to 300 °C. Since no deteriorations were found in either STA thin film, the TSC measurement was carried out.

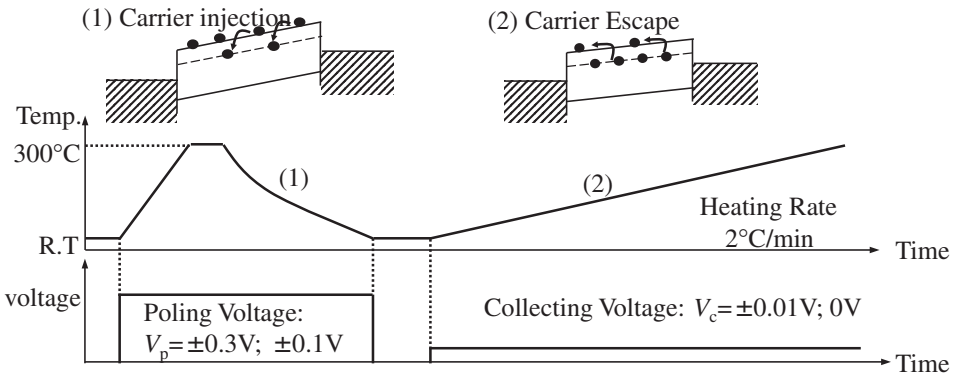

Fig. 1. TSC measurement profile.

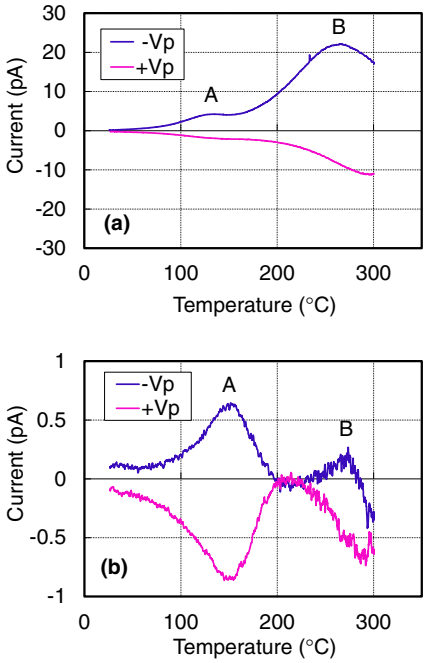

Fig. 2. (Color online) TSC diagrams of (a) STA-700 and (b) STA-800 measured in air when $+V_p$ and $-V_p$ were applied.

3. Results and Discussion

Figures 2(a) and 2(b) show the TSC profiles of the STA-700 and STA-800 measured in air, respectively. In both thin films, two TSC peaks were observed at low temperatures of approximately 130–150 °C, and two TSC peaks were observed at high temperatures of approximately 270–300 °C. This indicated that similar defect states existed in the two thin films. The defect that caused the TSC peaks at low temperatures will be called defect A, and the defect that caused the TSC peaks at high temperatures will be called defect B. However, the peaks observed at high temperatures were much stronger than the peaks observed at low temperatures in STA-700. In contrast, stronger peaks were observed at low temperatures in STA-800. Trap density and activation energy were calculated by the curve fitting of the TSC using the equation[24,25]

$$I_{TSC} = I_0 \exp\left[-\frac{E_t}{kT} - \frac{\nu}{\beta}\int_{T_0}^{T} \exp\left(-\frac{E_t}{kT}\right)dT\right], \quad (1)$$

where E_t is the activation energy, ν is the escape frequency factor, and β is the heating rate. The calculated activation energies of defects A and B were about 0.3 and 0.5 eV, respectively. The trap densities of defect A in STA-700 and STA-800 were about 0.2×10^{19} and $0.5 \times 10^{19}\,cm^{-3}$, respectively. A higher density of defect A was found in STA-800. The trap density of defect B in STA-700 was about $2.8 \times 10^{19}\,cm^{-3}$. This was much higher than densities of defect A in both thin films. Since the TSC peaks caused by defect B in STA-800 were very weak or very close to the highest measurement temperature of 300 °C, the trap densities were difficult to calculate accurately. However, these peaks were much weaker than the peaks observed at low temperatures. Therefore, the densities of defect B in STA-800 should be lower than those in STA-700. On the other hand, it was found that the TSC profiles were asymmetrical when the $+V_p$ and $-V_p$ were applied to the thin films.

In order to understand the above defects, the impurities in the thin films were investigated using SIMS. The depth profiles of various elements are shown in Fig. 3. Lower concentrations of C and H impurities were observed in STA-800 than in STA-700. A Ti impurity was detected in both thin films. This Ti was considered to diffuse from the TiO_2 layer under the bottom Pt electrode. In STA-700, the detected Ti was in the area close to the bottom interface. In STA-800, a higher concentration of Ti was observed and Ti diffused in the whole thin film. It was readily apparent that the distributions of Ti were nonuniform in both thin films. Since a higher density of defect A was observed in STA-800, we suggested that defect A is a Ti-related defect, and defect B is related to the C and H impurities. In our previous work, the electron energy-loss spectroscopy mapping of transmission electron microscopy showed that the diffused Ti mainly existed at grain boundaries in crystalline $BaTa_2O_6$ thin films.[17] Therefore, diffused Ti defects might have also existed in the STA thin films as Ti^{4+}. On the other hand, some researchers reported that the Ta in Ta_2O_5 could be replaced with Ti,[7] so that a small portion of diffused Ti might have also substituted for Ta in the STA matrix and generated Ti^{-} in our research. The asymmetry characteristics of the TSC peaks that were referred to above might be due to the different states of the top and bottom electrode/STA interfaces, because the impurity concentrations are different in the areas close to the two interfaces in the STA

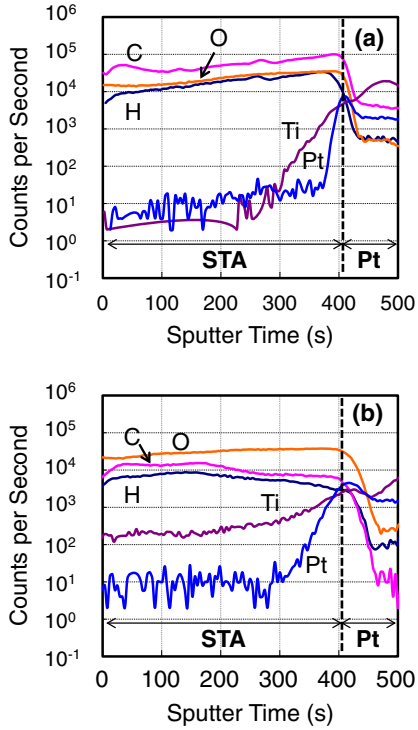

Fig. 3. (Color online) Depthwise profiles of various elements in (a) STA-700 and (b) STA-800.

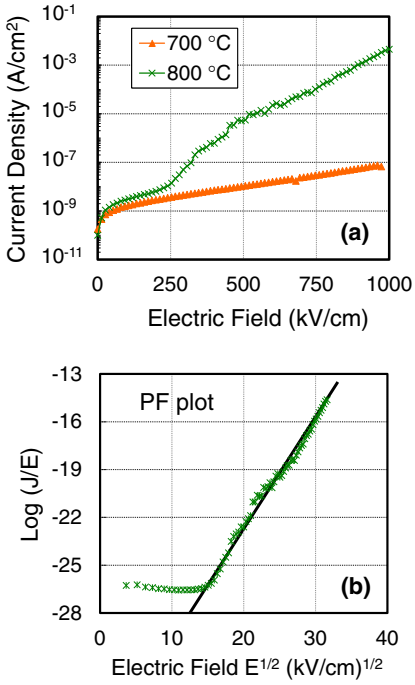

Fig. 4. (Color online) (a) Leakage current properties of STA-700 and STA-800. (b) Poole–Frenkel fitting plot of STA-800.

thin films. A continuous study should be carried out to clearly understand the state of Ti impurities, as well as the asymmetry through the changes in electrode material, substrate, and film thickness among others.

The leakage current properties of these two thin films were investigated, as shown in Fig. 4(a). At lower electrical fields, STA-800 showed a slightly larger leakage current than STA-700. However, at higher electrical fields, the leakage current was much larger in STA-800. To determine the dominant leakage current mechanism at higher electrical fields in STA-800, Poole–Frenkel (PF) analysis using the following equation was carried out:[19,22,27,28)]

$$J \propto E \exp\left[\frac{q\left(-\Phi_B + \sqrt{\frac{qE}{\pi\varepsilon_0\varepsilon_{op}}}\right)}{kT}\right], \quad (2)$$

where J denotes the current density, T represents the absolute temperature, k is the Boltzmann constant, q denotes the electronic charge, E represents the electric field, Φ_B is the barrier height of the trap, ε_0 is the dielectric constant of vacuum, and ε_{op} denotes the dynamic dielectric constant of the insulator material. A good linear fit was obtained in the PF plot, as shown in Fig. 4(b). If the calculated n using $\varepsilon_{op} = n^2$ from the slope of the fitted line is the same as the experimental n, the leakage current can be determined by the PF mechanism.[22,28,29)] The calculated n was 1.5, which was in good agreement with that (1.8–2.2) measured by spectroscopic ellipsometry. Thus, the PF mechanism was considered to dominate in STA-800 at higher electrical fields. This suggested that moving electrons were trapped in the thin film by defect states and that a much larger leakage current occurred at higher electric fields. As we discussed above, a higher density of defect A was found in STA-800. Therefore, we suggested that the larger leakage current in STA-800 was mainly caused by this higher density of defect A, i.e., the Ti impurity mainly caused the leakage current of STA thin films.

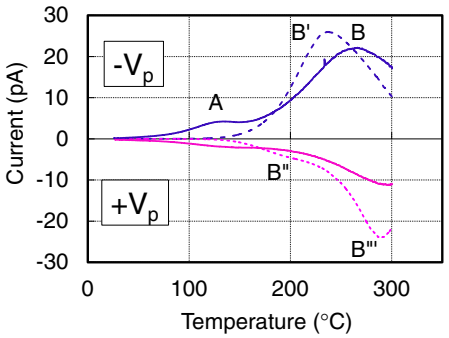

Fig. 5. (Color online) TSC diagrams of STA-700 measured in air (solid lines) and vacuum (dashed lines).

It is well known that oxygen vacancies play an important role in oxide thin films.[9)] In many reports, oxygen vacancies in oxide materials can be generated while annealing in vacuum.[30,31)] Therefore, STA-700 was also measured in vacuum for further investigation. In consideration of the low-pressure measurement atmosphere of TSC and the increase in measurement temperature (the measurement temperature was over 250 °C, held for about 1 h), more oxygen vacancies were expected to be generated and oxygen-vacancy-related defects were easily observed. The TSC profiles, which were measured in air and vacuum are compared, in Fig. 5. Different peaks were observed when the thin film was measured in vacuum. A TSC peak was found at a temperature lower than 270 °C when $-V_p$ was applied. The defect that caused this peak will be called B′. Two other

peaks were clearly observed at approximately 200 and 290 °C when $+V_p$ was applied. The defects that caused these two peaks will be called B″ and B‴, respectively. The calculated activation energy of defect B‴ was about 0.8 eV, which was the same as the energy of the first ionization of the oxygen vacancy deep double donor reported by Lau *et al.* and Sawada *et al.*[6,9] Moreover, this peak was observed in an environment in which oxygen vacancies were easily generated. Thus, we thought that defect B‴ was an oxygen-vacancy-related defect. Lau *et al.* also pointed out oxygen vacancy double donors could be singly and doubly ionized to V_o^+ or V_o^{++}. V_o^+ could attract ionized C^- and H^- to generate relatively shallow single donors, C^-–V_o^+ and H^-–V_o^+.[6–8] In their reports, the activation energies of the generated C^-–V_o^+ and H^-–V_o^+ shallow donors were about 0.49–0.57 eV, which were close to those of defects B′ and B″ (0.5–0.6 eV). Therefore, we thought that the same phenomenon might have occurred in our thin film, and that defects B′ and B″ originated from the combination of C and H impurities with oxygen vacancies. These results also reinforced our hypothesis that defect B is related to the C and H impurities. Although oxygen-vacancy-related defects could not be clearly observed by the TSC measurement in air, it was clearly observed in vacuum. This suggests that most defects in STA thin films could be easily observed by further improving TSC measurement conditions.

It was also found that the TSC peaks caused by defect A disappeared when the thin film was measured in vacuum. While the thin film was measured in air, some H_2O or other impurities from air could have been adsorbed onto the thin film when voltage was applied.[32] On the other hand, when the thin film was measured in vacuum, more oxygen vacancies were expected to be generated in the thin film. Therefore, the disappearance of the peaks might be affected by the environment or oxygen vacancies. Further research will be carried to solve this problem.

4. Conclusions

In this research, we demonstrated that defect states in sol–gel derived STA thin films can be detected by a TSC technique. We also tentatively explained leakage current properties using these defect states. Similar defect states were found in STA-700 and STA-800 thin films by TSC investigation. It was suggested that the TSC peaks observed at low temperatures might have been caused by the Ti impurity, and that the TSC peaks observed at high temperatures might have been caused by the C and H impurities. Ti-related defects were likely to contribute mainly to the leakage current of STA thin films. Thus, a larger leakage current was observed in STA-800 which contained more Ti impurities. Oxygen-vacancy-related defects were also clearly observed when the STA thin films were measured in vacuum. It is thus expected that most defects in STA thin films will be easily observed by improving measurement conditions. Continuous research, such as on the change in electrode material, substrate, film thickness, and measurement atmosphere, is necessary for further understanding of various defects in STA thin films.

Acknowledgements

We are thankful for the support in the form of a Grant-in-Aid for Young Scientists (B) to the Ministry of Education, Culture, Sports, Science and Technology, Japan, and for a Grant-in-Aid for Ph. D. students (NAIST).

1) A. I. Kingon, J.-P. Maria, and S. K. Streiffer: Nature **406** (2000) 1032.
2) K. Kishiro, N. Inoue, S.-C. Chen, and M. Yoshimaru: Jpn. J. Appl. Phys. **37** (1998) 1336.
3) S. Ezhilvalavan and T.-Y. Tseng: J. Appl. Phys. **83** (1998) 4797.
4) W. S. Lau, K. K. Khaw, P. W. Qian, N. P. Sandler, and P. K. Chu: Jpn. J. Appl. Phys. **35** (1996) 2599.
5) W. S. Lau, K. K. Khaw, P. W. Qian, N. P. Sandler, and P. K. Chu: J. Appl. Phys. **79** (1996) 8841.
6) W. S. Lau, L. L. Leong, T. Han, and N. P. Sandler: Appl. Phys. Lett. **83** (2003) 2835.
7) W. S. Lau, T. S. Tan, P. Babu, and N. P. Sandler: Appl. Phys. Lett. **90** (2007) 112903.
8) W. S. Lau, K. K. Khaw, T. Han, and N. P. Sandler: Appl. Phys. Lett. **89** (2006) 262901.
9) H. Sawada and K. Kawakami: J. Appl. Phys. **86** (1999) 956.
10) S. Regnery, R. Thomas, P. Ehrhart, and R. Waser: J. Appl. Phys. **97** (2005) 073521.
11) W.-J. Lee, I.-K. You, S.-O. Ryu, B.-G. Yu, K.-I. Cho, S.-G. Yoon, and C.-S. Lee: Jpn. J. Appl. Phys. **40** (2001) 6941.
12) M. Silinskas, M. Lisker, B. Kalkofen, and E. P. Burte: Mater. Sci. Semicond. Process. **9** (2006) 1102.
13) D.-O. Lee, P. Roman, C.-T. Wu, P. Mumbauer, M. Brubaker, R. Grant, and J. Ruzyllo: Solid-State Electron. **46** (2002) 1671.
14) E. Tokumitsu, G. Fujii, and H. Ishiwara: Appl. Phys. Lett. **75** (1999) 575.
15) E. Tokumitsu, K. Okamoto, and H. Ishiwara: Jpn. J. Appl. Phys. **40** (2001) 2917.
16) B.-G. Chae, W.-J. Lee, I.-K. You, S.-O. Ryu, M.-Y. Jung, and B.-G. Yu: Jpn. J. Appl. Phys. **41** (2002) L729.
17) L. Lu, T. Nishida, M. Echizen, K. Uchiyama, and Y. Uraoka: Jpn. J. Appl. Phys. **49** (2010) 09MA14.
18) L. Lu, Y. Miura, T. Nishida, M. Echizen, Y. Ishikawa, K. Uchiyama, and Y. Uraoka: Jpn. J. Appl. Phys. **51** (2012) 03CB05.
19) L. Lu, T. Nishida, M. Echizen, K. Uchiyama, and Y. Uraoka: Thin Solid Films **520** (2012) 3620.
20) W. Sakamoto, Y.-S. Horie, T. Yogo, and S.-I. Hirano: Jpn. J. Appl. Phys. **40** (2001) 5599.
21) Y. Hamazaki, W. Sakamoto, M. Moriya, and T. Yogo: Jpn. J. Appl. Phys. **48** (2009) 09KA08.
22) B. Miao, R. Mahapatra, N. Wright, and A. Horsfall: J. Appl. Phys. **104** (2008) 054510.
23) Y. H. Lee, T. W. Kang, and T. W. Kim: J. Appl. Phys. **71** (1992) 5419.
24) T. Nishida, M. Matsuoka, S. Okamura, and T. Shiosaki: Jpn. J. Appl. Phys. **42** (2003) 5947.
25) R. R. Haering and E. N. Adams: Phys. Rev. **117** (1960) 451.
26) T. P. Juan, S. Chen, and J. Y. Lee: J. Appl. Phys. **95** (2004) 3120.
27) T. Nozaka, Y. Mizutani, B. Gun, M. Echizen, T. Nishida, H. Takeda K. Uchiyama, and T. Shiosaki: Jpn. J. Appl. Phys. **47** (2008) 7494.
28) F.-C. Chiu, J.-J. Wang, J. Y. Lee, and S. C. Wu: J. Appl. Phys. **81** (1997) 6911.
29) K.-H. Cho, C.-H. Choi, J.-Y. Choi, T.-G. Seong, S. Nahm, C.-Y. Kang, S.-J. Yoon, and J.-H. Kim: J. Eur. Ceram. Soc. **30** (2010) 513.
30) N. Zhong, S. Okamura, K. Uchiyama, and T. Shiosaki: Appl. Phys. Lett. **87** (2005) 252901.
31) S.-J. Seo, Y. H. Hwang, and B.-S. Bae: Electrochem. Solid-State Lett. **13** (2010) H357.
32) J.-S. Park, J. K. Jeong, H.-J. Chung, Y.-G. Mo, and H. D. Kim: Appl. Phys. Lett. **92** (2008) 072104.